https://doi.org/10.1016/j.scriptamat.2020.05.008

Breaking the strength-ductility paradox in advanced nanostructured Fe-based alloys through combined Cu and Mn additions

H.J. Kong [a], T. Yang [a], R. Chen [b], S.Q. Yue [c], T.L. Zhang[c], B.X. Cao [c], C. Wang [c], W.H. Liu[d], J.H. Luan[c,e], Z.B. Jiao[f], B.W. Zhou [g], L.G. Meng[g], A. Wang [c], C.T. Liu[a,c,e,□]

[a] Department of Mechanical Engineering, City University of Hong Kong, China

[b] School of Mechanical Engineering and Electronic Information, China University of Geosciences, Wuhan 430074, China

[c] Department of Materials Science and Engineering, City University of Hong Kong, China

[d] School of Materials Science and Engineering, Harbin Institute of Technology (Shenzhen), China

[e] Center for Advanced Structural Materials, Department of Mechanical Engineering, City University of Hong Kong, China

[f] Department of Mechanical Engineering, The Hong Kong Polytechnic University, Hong Kong, China

[g] School of Materials Science and Engineering, Dalian University of Technology, Dalian 116024, China

Abstract

The strength-ductility paradox is a long-sought challenge for all engineering materials. In this study, we escaped the strength-ductility trade-off by engineering nano-scale heterogeneities carefully in the advanced nanostructured Fe-based alloys through alloying with Cu and Mn additions. We demonstrated a triple ductility enhancement by 20% together with a strength improvement of 100MPa compared to the alloys with sole Cu additions, overturning a common understanding of the strength-ductility trade-off. The strength-ductility enhancement is attributed to the complex interplay between the

transformation induced plasticity (TRIP) and the coherent nano-scale Cu precipitates as well as the resultant heterogeneous stress–strain partitioning and dislocation interactions.

Nanostructured Fe-based alloys with a superior strength and ductility are desperately needed in various engineering sectors such as the automotive, construction, naval, and energy industries due to the recent urge to mitigate the global carbon emission [1–8]. The strength-ductility paradox is often a common dilemma during the design of the high strength nanostructured iron-based alloys. This is not exclusively for the Fe-based alloys but a prominent problem for all engineering materials. On the other hand, the nature seems to have its own remedy to deal with the strengthductility trade-off. Nacre and bone are the two naturally occurring materials that are made up of brittle fundamental blocks but possess exceptional toughness due to their intriguing heterogeneous structures [9].

Tremendous efforts have been put forth by several research groups [10–13] to break the strength-ductility limit of the nanostructured Fe-based alloys by engineering heterogeneities. Nevertheless, their approaches rely on a high level of carbon (C > 0.15 wt%), nickel (Ni >3 wt%), and manganese (Mn >8wt%) additions that compromise the alloys' weldability and cost effectiveness. Our previous work [14, 15] showed that the additions of Cu can produce cheap weldable low carbon iron-based alloys with a good strength (Yield strength: YS ~1000 MPa, Ultimate tensile strength: UTS ~1200 MPa)

and satisfactory ductility (Total Elongation: TE ~10 %). In this work, we demonstrate that through the combined additions of Cu and Mn, the strength and ductility can be further improved by 100MPa and 20% (triple our previous work [14, 15] with only Cu additions) respectively, breaking the conventional strength-ductility paradox! The synergistic effects of the combined Cu and Mn additions on the strength-ductility balance are two-fold: i) Mn additions promote the formation of nanoscale (~300–500 nm) reversed austenite grains, especially important for the transformation induced plasticity (TRIP) effect and ii) Cu additions provide strengthening through the formation of coherent nanoscale precipitates and additional ductilizing mechanisms by creating a more heterogeneous strain partitioning as well as a more progressive TRIP effect.

The starting alloy with a nominal composition of Fe–8Mn–1Ni–2Cu–3Cr–1.1Si–0.8Mo–0.5Al–0.3Ti–0.11C–0.02B, wt% was melted in a vacuum induction melting furnace. The cast ingot was hot rolled at 1000 and 900℃ to a respective thickness of 10 and 3mm, followed by 60% cold roll reduction to a final thickness of 1mm. In order to obtain nanostructured alloy samples with superb strength-ductility balance, the alloy sheet was subjected to various heat treatments listed in Table 1. Tensile tests were performed on wire cut specimens with a gauge length of 12.5mm and a cross section of 3.2 × 1 mm at a strain rate of 0.001/s. The microstructural analyses were performed with scanning electron microscopy (SEM) based electron back scattered diffraction (EBSD) at a step size of 0.02μm as well as the atom probe tomography (APT) with detailed parameters described in our previous work [15].

The tensile properties of our nanostructured alloy samples after different heat treatments are tabulated in Table 2. For a better representation, some stress–strain curves are selectively plotted in Fig. 1. The 700℃ WQ sample (Roll 60% + 700℃ 10-min water quenched) showed YS ~900MPa, UTS ~1482MPa and total elongation ~13% with an initial rapid work hardening. The EBSD analyses (Table 3) reveal a mixture of FCC and BCC phase fractions of 22% and 78%, respectively. The FCC phase is distributed along the BCC grain boundaries and resembles islandlike morphology (Fig. 2a and b), indicating the presence of retained austenite. During the short 10-min 700 °C annealing, nanometer-sized (~300–500nm) austenite grains formed from the cold rolled sample through nucleation and growth while some ferrite grains also formed due to recrystallization. The nanometer-sized austenite grains transformed into martensite during the quenching of the sample. At the same time, internal stress built up, stabilizing the remaining untransformed austenite phase and resulted in the formation of islandlike retained austenite. The presence of the martensite during the quenching from 700℃ is supported by its higher YS compared to the 700℃ furnace cooled (700℃ FC) sample. Moreover, from the EBSD analyses (Fig. 2a and b), two types of BCC grains can be observed: large (~1μm) elongated BCC grains and nanometer-sized (300–500nm) equiaxed BCC grains. The large elongated BCC grains are believed to be the partially recrystallized ferrite grains [16]. Meanwhile, the nanometer-sized equiaxed BCC grains are martensite formed during the 700℃ quenching. The large initial work hardening is attributed to the rapid dislocation multiplications due to the strain partitioning between the hard and soft phases such as the hard martensite and soft ferrite [17]. Apart from

this, the transformation of the austenite to martensite (TRIP) as well as the generation of stacking faults, partial dislocations, and twins during tensile deformation can also give extra contribution to the high work hardening [12, 18].

With a subsequent low temperature single step annealing at 640℃ 10-min followed by water quenching (LTSS: Roll 60% + 700℃ 10-min WQ+ 640℃ 10-min WQ), the sample showed an astounding ductility improvement by almost twice from the total elongation of 15% in the 700℃ WQ sample to the total elongation of 25%. Besides, the 640℃ WQ annealed sample showed a large Lüder's deformation (characterized by zero work hardening plateau) at the initial stage of tensile deformation followed by a slow and gradual work hardening until the onset of necking, as depicted in Fig. 1. The Lüder's deformation will be explained further in this text later. The slow and gradual work hardening is attributed to the formation of stable nanometer-sized (~300–500 nm, as shown in Fig. 2 c and d) reversed austenite during the low temperature 640℃ annealing. Different from the rapid work hardening in the 700℃ annealed sample, the stable reversed austenite after the 640℃ annealing allows a more gradual TRIP effect, ensuring a slow but continuous stress release that avoids excessive stress build-up at the grain boundaries during deformation and thus enhanced ductility [13, 19,20]. From the EBSD analyses (Table 3) the austenite area fraction increases from 22% in the 700℃ WQ sample to 33% after the 640℃ annealing, indicating the nanometer-sized reversed austenite formed during the low temperature 640℃ annealing is more stable against martensite transformation than that of the 700℃ high temperature annealing. The austenite formed during the high temperature 700℃

annealing is unstable against the martensite transformation due to the low content of austenite stabilizers such as Mn, Ni, Cu, and C [21]. The subsequent water quenching resulted in the formation of martensite supersaturated with the austenite stabilizers [22]. To relieve the supersaturation, these austenite stabilizers will partition to the newly formed reversed austenite or form Cu precipitates or carbides during the 640℃ annealing. From the APT analyses (Fig. 3), obvious Mn partitioning (~15 wt%) in the austenite phase can be observed. Besides, Ni, Cu and C atoms were also found weakly partitioned into the austenite phase, about 1.37 wt%, 0.68 wt%, and 0.03 wt%, respectively. Consequently, the austenite formed after the 640℃ annealing is more stable against marten- sitic transformation. The Cu precipitation was hardly detected in the APT analyses, suggesting Cu atoms have a higher tendency to partition into the austenite than being precipitated out as Cu pre- cipitates. It is very interesting to note that the 640 °C annealed sample has the same YS as that of the 700℃ WQ sample. The 640℃ annealing should have softened the martensite formed during the 700℃ WQ, indicating the presence of other strengthening mechanisms. The strengthening can come from the carbide precipitation or/and the stabilized austenite phase after the 640℃ annealing. The stabilized austenite is generally harder as a higher stress is required to initiate yielding and the subsequent TRIP effect [23, 24]. One might also argue that martensite might have formed during the 640℃ quenching and subsequently strengthened the sample. For this reason, tensile tests were performed on the 640℃ WQ and 640℃ FC samples. Both the samples showed similar mechanical properties (YS

~1150 MPa, UTS ~1250MPa, TE ~25%), suggesting no formation of a martensite during the 640°C water quenching.

In order to further improve the mechanical performances of the nanostructured alloy, the 700°C WQ sample was subjected to a low temperature double-step annealing treatment (LTDS: Roll 60% + 700°C 10-min WQ + 640°C 10-min WQ + 500°C 2h WQ). The results were very encouraging such that both the YS and total elongation of the sample were further improved from ~900MPa to ~1100MPa and ~15% to 30% (ductility enhancement by twice), respectively, breaking the conventional strength-ductility paradox! The APT analyses (Fig. 4) revealed ultrafine nanoscale (~3–4nm) Cu precipitation along the grain-boundary regions, instead of the commonly reported homogeneous distribution throughout the BCC alloy matrix. This can be understood as our nanostructured samples consist of fine nanometer-sized (~300–500nm) grains and contain a high interfacial energy. To reduce such a high interfacial energy, grain boundary precipitation is thus more favored. Different from the conventional large and brittle grain boundary precipitates that often serve as stress conservators deteriorating the mechanical properties of alloys, these ultrafine nanoscale Cu precipitates are soft and maintain high coherency with the alloy matrix that allows dislocations to shear through without initiating cracks. The strengthening and work hardening due to the Cu precipitates can be explained from three perspectives. Firstly, the Cu precipitates improve the yield strength by pinning the dislocations due to the difference in the elastic modulus between the Cu precipitates and the -Fe matrix in accordance to the Russel-Brown dislocation shearing model [25]. This precipitate shearing mechanism will not

contribute to significant work hardening. Secondly, the Cu precipitates can also contribute to strengthening by increasing the hardness of the nanometer-sized low temperature reversed austenite. The Cu precipitates increase the hardness of the reversed austenite or its stability against martensitic transformation by supressing the shape change during the transformation, leading to a more gradual release of TRIP effect or a more progressive work hardening [23, 24]. Thirdly, the Cu precipitates create a more heterogeneous strain partitioning that encourages a better dislocation accumulation through the generation of geometrical necessary dislocations, resulting in the formation of long-range back stresses and enhanced yield strength as well as the improved work hardening [26–31]. The Cu precipitates at the grain boundaries can also help in strengthening the grain boundaries or stress transfer by imposing a strong barrier that prevents stress concentration due to dislocation thickening at the grain boundaries [26, 27]. Since the carbon concentration of the alloy matrix did not show much variation between the double step (Fig. 4b) and single step (Fig. 3b) annealed samples, the strengthening due to carbide precipitation after the double step annealing can be considered insignificant.

The double step annealed sample demonstrated a similar stress–strain behavior as in the single step 640℃ annealed sample but with improved the Lüder's stress (by 100MPa), a longer Lüder's strain (by 4 %), and larger yield drop (by 50MPa). To have a better understanding on the Lüder's strain enhancement, EBSD analyses were performed on the double step annealed specimen after tensile strained for 5%, as shown in Fig. 2g and h. The austenite phase fraction decreased from the initial 51% to 21%

(Table 3), indicating TRIP occurred during the Lüder's deformation. However, according to the conventional understanding, the TRIP effect should have also resulted in the enhanced work hardening and yet zero work hardening Lüder's plateau was observed. The Lüder's deformation is a localized nonuniform plastic deformation that is usually initiated at one end and propagates to the other end of the sample. Owing to the extremely fine grain size (~300–500 nm) in our nanostructured samples, dislocations hardly develop and thus reduces the sample's ability to work harden [26–27, 32]. This often results in the early onset of the plastic instability or necking. The TRIP effect provides work hardening in our nanostructured samples to compensate the stress concentration attributed to the area reduction at the propagating front due to the plastic instability and hence the development of a stable Lüder's strain with zero work hardening plateau. As the work hardening exceeds that is required to compensate the area reduction, the Lüder's strain get exhausted and the normal uniform deformation takes place with a positive work hardening. The longer Lüder's plateau or Lüder's strain at a higher yield strength can be attributed to a more stable austenite phase, leading to a more gradual TRIP effect that provides just enough martensite to counterbalance the area reduction [33]. Different from the previously reported stabilizing effect through the partitioning of austenite stabilizers such as Mn and C [10, 21, 34–35], our APT analyses (Fig. 4b) revealed that Mn partitioning in the austenite reduces after the double stage treatment, perhaps due to the increased austenite fraction [21]. The improved austenite stability in this present work most probably comes from the nanoscale Cu precipitation at grain boundaries. These nanoscale Cu precipitates sitting on the grain

boundaries can suppress the martensitic transformation by obstructing the shape change during the transformation. In other words, the nanoscale Cu precipitation can serve as a complementary approach to stabilize the austenite apart from relying solely on C and Mn that are undesirable in the industry. The higher Lüder's stress also supports the formation of more stable reversed austenite grains as a higher stress is needed to initiate the TRIP transformation. The large yield drop can be probably attributed to the lack of mobile dislocations due to dislocation recovery after the double step annealing [13, 36] .

In essence, a strong yet ductile advanced nanostructured Fe- based alloy (YS: 1100MPa, UTS: 1300MPa, TE: 30%) containing Cu and Mn additions has been developed through the double-step low-temperature annealing. Nanoscale (~3–4nm) coherent grain boundary Cu precipitation together with the formation of stable nanometre-sized (~300–500nm) reverse austenite can lead to both strength and ductility improvement in nanostructured Fe-based alloys, breaking the conventional strength-duccility trade-off. Furthermore, the gradual TRIP effect allows a more controlled work hardening leading to a dramatic Lüder's strain and ductility improvement.

Declaration of Competing Interest

The authors declare that they have no known competing finan- cial interests or personal relationships that could have appeared to influence the work reported in this paper.

Acknowledgment

The authors gratefully acknowledge the financial support of the City University of Hong Kong through the CityU grant 9360161.

References

1 Z.B. Jiao, J.H. Luan, M.K. Miller, Y.W. Chung, C.T. Liu, Mater. Today 20 (3) (2017) 142.

2 Y.R. Wen, A. Hirata, Z.W. Zhang, T. Fujita, C.T. Liu, J.H. Jiang, M.W. Chen, Acta Mater. 61 (2013) 2133.

3 M.E. Fine, S. Vaynman, D. Isheim, Y.W. Chung, S.P. Bhat, C.H. Hahin, Metall. Mater. Trans. A 41 (2010) 3318.

4 S. Vaynman, D. Isheim, R.P. Kolli, S.P. Bhat, D.N. Seidman, M.E. Fine, Metall. Mater. Trans. A 39 (2008) 363.

5 G. Song, Z. Sun, L. Li, X. Xu, M. Rawlings, C.H. Liebscher, B. Clausen, J. Poplawsky, D.N. Leonard, S. Huang, Z. Teng, C.T. Liu, M.D. Asta, Y. Gao, D.C. Dunand, G. Ghosh, M. Chen, M.E. Fine, P.K. Liaw, Sci. Rep. 5 (2015) 16327.

6 M. Kapoor, D. Isheim, G. Ghosh, V. S, M.E. Fine, Y.W. Chung, Acta Mater. 73 (2014) 56.

7 S.S. Xu, J.P. Li, Y. Cui, Y. Zhang, L.X. Sun, J. Li, J.H. Luan, Z.B. Jiao, X.L. Wang, C.T. Liu, Z.W. Zhang, Int. J. Plast. 128 (2020) 102677.

8 D. Suh, S. Kim, Scr. Mater. 126 (2017) 63.

9 G. Gu, F. Libonati, S.D. Wettermark, M.J. Buehler, J. Mech. Behav. Biomed. 67 (2017) 135.

10 B.B. He, B. Hu, H.W. Yen, G.J. Cheng, Z.K. Wang, H.W. Luo, M.X. Huang, Science 357 (6355) (2017) 1029.

11 S. Jiang, H. Wang, Y. Wu, X. Liu, H. Chen, M. Yao, B. Gault, D. Ponge, D. Raabe, A. Hirata, M. Chen, Y. Wang, Z. Lu, Nature 544 (2017) 460.

12 M.M. Wang, C.C. Tasan, D. Ponge, D. Raabe, Acta Mater. 111 (2016) 262.

13 S. Gao, Y. Bai, R. Zheng, Y. Tian, W. Mao, A. Shibata, N. Tsuji, Scr. Mater. 159 (2019) 28.

14 Z.B. Jiao, J.H. Luan, Z.W. Zhang, M.K. Miller, W.B. Ma, C.T. Liu, Acta Mater. 61 (16) (2013) 5996.

15 H.J. Kong, C. Xu, C.C. Bu, C. Da, J.H. Luan, Z.B. Jiao, G. Chen, C.T. Liu, Acta Mater. 172 (2019) 150.

16 Y. Ma, W. Song, S. Zhou, A. Schwedt, W. Bleck, Metals 8 (5) (2018) 357.

17 M. Calcagnotto, Y. Adachi, D. Ponge, D. Raabe, Acta Mater. 59 (2011) 658.

18 M.M. Wang, C.C. Tasan, D. Ponge, A. Kostka, D. Raabe, Acta Mater. 79 (2014) 268.

19 J. Hu, W. Cao, C. Wang, H. Dong, J. Li, ISIJ Int. 54 (8) (2014) 1952.

20 J. Liu, C. Chen, Q. Feng, X. Fang, H. Wang, F. Liu, J. Lu, D. Raabe, Mater. Sci. Eng. A 703 (2017) 236.

21 B. Sun, F. Fazeli, C. Scott, B. Guo, C. Aranas Jr, X. Chu, M. Jahazi, S. Yue, Mater. Sci. Eng. A 729 (2018) 496.

22 M.K. Banerjee, Elsevier, Canada, 2016, p. 1.

23 O. Muransky, P. Sittner, J. Zrnik, E.C. Oliver, Acta Mater. 56 (2008) 3367.

24 S. Morito, K. Oh-Ishi, K. Hono, T. Ohba, ISIJ Int. 51 (7) (2011) 1200.

25 K.C. Russel, L.M. Brown, Acta Metall. 20 (7) (1972) 969.

26 Y.T. Zhu, X.L. Wu, Mater. Today Nano 2 (2018) 15.

27 S. Lee, S.J. Lee, B.C.D. Cooman, Acta Mater. 59 (2011) 7546.

28 J.H. Ryu, D.I. Kim, H.S. Kim, H.K.D.H. Bhadeshia, D.W. Suh, Scr. Mater. 63 (2010) 297.

29 B. Sun, F. Fazeli, C. Scott, X. Yan, Z. Liu, X. Qin, S. Yue, Scr. Mater. 130 (2017) 49.

30 X.L. Liu, Q.Q. Xue, W. Wang, L.L. Zhou, P. Jiang, H.S. Ma, F.P. Yuan, Y.G. Wei, X.L. Wu, Materialia 7 (2019) 100376.

31 M.X. Yang, F.P. Yuan, Q.G. Xie, Y.D. Wang, E. Ma, X.L. Wu, Acta Mater. 109 (2016) 213.

32 N. Tsuji, Y. Ito, Y. Saito, Y. Minamino, Scr. Mater. 47 (2002) 893.

33 J.H. Ryu, J.I. Kim, H.S. Kim, C. Oh, H.K.D.H. Bhadeshia, D. Suh, Scr. Mater. 68 (2013) 933.

34. D.Raabe, S. Sandlobes, J. Millan, D. Ponge, H. Assadi, M. Herbig, P.P. Choi, Acta Mater. 61 (2013) 6132.

35 Z.H. Cai, H. Ding, H. Kamoutsi, G.N. Haidemenopoulos, R.D.K. Misra, Mater. Sci. Eng. A 654 (2016) 359.

3C.Y. Yu, P.W. Kao, C.P. Chang, Acta Mater. 53 (2005) 4019.

Figure captions

Fig. 1. The selected stress–strain curves of the nanostructured iron-based alloy samples with different heat treatments. WQ: Water quench; LTSS: Low temperature single step; LTDS: Low temperature double step.

Fig. 2.EBSD analyses showing the band contrast and phase map of (a)(b) 700℃ WQ, (c)(d) LTSS (Roll 60% + 700℃ 10-min WQ + 640℃ 10-min WQ), (e)(f) LTDS (Roll 60% + 700℃ 10-min WQ + 640℃ 10-min WQ + 500℃ 2h WQ), and (g)(h) 5 % tensile strained LTDS. red: FCC phase; blue: BCC phase; orange: HCP phase, F: Ferrite, A: Austenite, M: Martensite.

Fig. 3. (a) The 3D-APT reconstruction and (b) the proximity histogram for the partitioning behavior in the austenite phase of the LTSS sample (Roll 60% + 700℃ 10-min WQ + 640℃ 10-min WQ).

Fig. 4. (a) The 3D-APT reconstruction together with the proximity histogram showing the (b) partitioning behavior in the austenite phase and (c) nanoscale Cu precipitates of the LTDS sample (Roll 60% + 700℃ 10-min WQ + 640℃ 10-min WQ + 500℃ 2h WQ). The 3D reconstruction with C and Cu superimposed was reoriented to show the grain boundary precipitation.

Fig 1

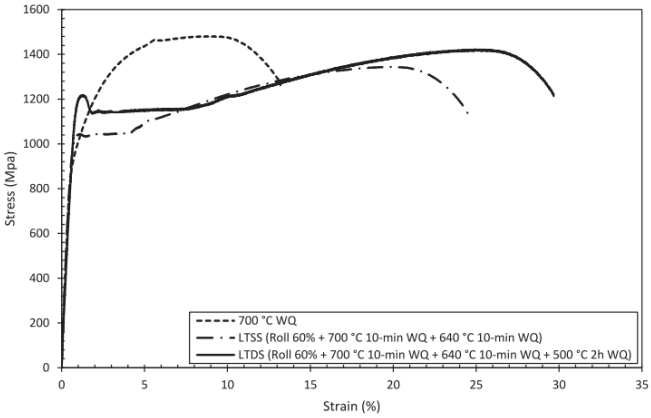
1600
1400
1200
1000
800
600
400
200
0
Stress (Mpa)
0
5
10
15
20
25
30
35
Strain (%)
700 °C WQ
LTSS (Roll 60% + 700 °C 10-min WQ + 640 °C 10-min WQ)
LTDS (Roll 60% + 700 °C 10-min WQ + 640 °C 10-min WQ + 500 °C 2h WQ)

Fig 2

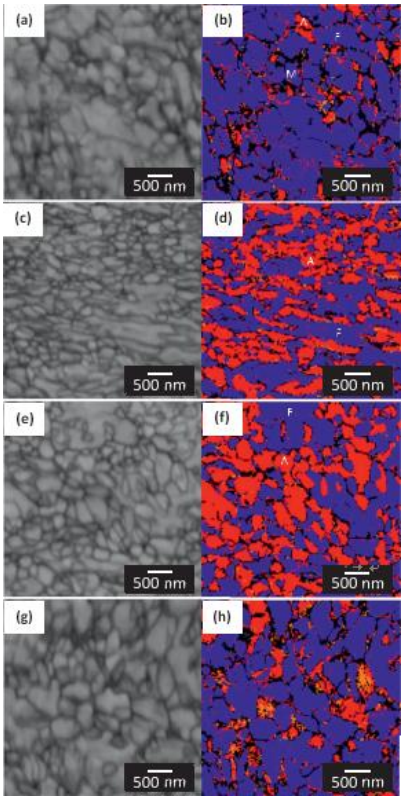
(a)
500 nm
(b)
M
500 nm
(c)
500 nm
(d)
A
F
500 nm
(e)
500 nm
(f)
F
A
500 nm
(g)
500 nm
(h)
500 nm

Fig 3

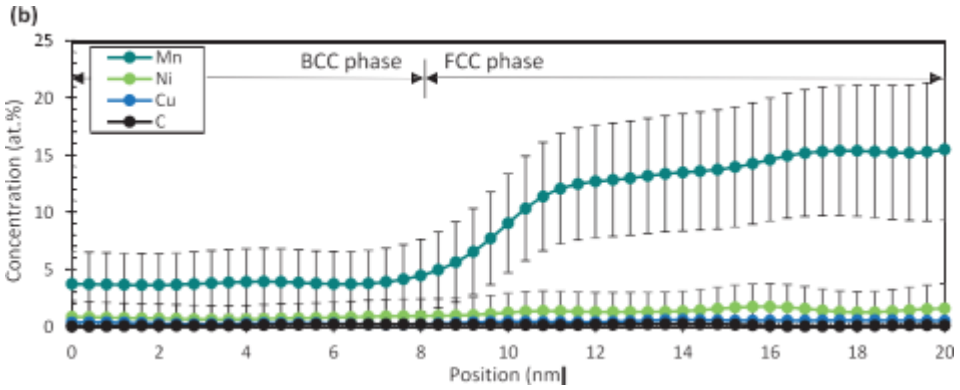
(b)
Mn
Ni
Cu
C
BCC phase
FCC phase
Concentration (at.%)
Position (nm)
0
5
10
15
20
25
0
2
4
6
8
10
12
14
16
18
20

Fig 4